

# Effect of Flow Regime on Convective Heat Transfer in Porous Copper Manufactured by Lost

## Carbonate Sintering

Xianke Lu and Yuyuan Zhao\*

School of engineering, University of Liverpool, Liverpool L69 3GH, UK

### Abstract

The fluid flow hydrodynamics and forced convective heat transfer in porous Cu samples manufactured by the Lost Carbonate Sintering process, with pore size 425-710  $\mu\text{m}$  and porosities 0.6-0.8, have been investigated experimentally. Pressure drop and heat transfer coefficient were measured for pore-based Reynolds numbers in the range of 0.5-380. Five flow regimes, namely pre-Darcy, transition to Darcy, Darcy, transition to non-Darcy and non-Darcy, were identified. The Reynolds numbers for the flow regime boundaries increased nearly linearly with porosity. The permeability of the porous Cu samples increased and the form drag coefficient decreased with increasing porosity. Both the friction factor and the heat transfer coefficient depended strongly on the flow rate. The relationship between Nusselt number and Reynolds number showed three sections, with each section fitting well with the correlation  $Nu = C_T Re^n$  with different  $C_T$  and  $n$  values. The value of  $n$  was largely independent of porosity, except at the lowest porosity. The flow regimes had a strong effect on the heat transfer performance. The three sections of the Nusselt number vs Reynolds number curves broadly corresponded to the pre-Darcy, Darcy and non-Darcy regimes.

Keywords: Porous metal, convective heat transfer, porous flow, flow regime, pressure drop.

\*Corresponding author

Professor Yuyuan Zhao

School of Engineering

University of Liverpool

Liverpool L69 3GH

UK

Email: yyzhao@liverpool.ac.uk

Tel.: +44 (0)151 794 4697

## 1. Introduction

Open cell porous metals show excellent heat transfer performance under forced convection conditions due to their large specific surface area and good fluid flow permeability (Ashby *et al.*, 2000; Goodall and Mortensen, 2014; Thewsey and Zhao, 2008). They are regarded as potential candidates for use in active cooling devices for high-rate heat dissipation, especially when conventional passive cooling techniques are inadequate (Hetsroni *et al.*, 2006). Pressure drop and heat transfer coefficient are two key parameters for their use as heat exchangers (Diani *et al.*, 2015; Nie *et al.*, 2017). Therefore, understanding the relationships between fluid flow hydrodynamics and heat transfer in porous metals under forced convection is of great significance for the development of new generation compact heat exchangers.

The relationship between pressure drop and flow velocity in porous media was firstly correlated by Darcy (Bejan, 2013) based on experimental observations. He found that the cross-sectional averaged velocity through a column of porous medium is proportional to the pressure drop along the porous material and inversely proportional to the viscosity of the working fluid. Darcy's law is normally expressed as follows:

$$\frac{\Delta P}{L} = -\frac{\mu}{K}V \quad (1)$$

where  $\Delta P$  is the pressure drop,  $L$  is the length of the sample,  $\mu$  is the viscosity of the fluid,  $K$  is the permeability of the porous medium, and  $V$  is the Darcian velocity, which is the volumetric flow rate of the fluid divided by the cross-sectional area.

Unfortunately, Darcy's law is only applicable to very slow moving flows in a quite narrow Reynolds number range. Deviation from the Darcy law is observed when the Reynolds number exceeds a certain value depending on the porous medium's structure and characteristic length, due to the effects of inertial force. Forchheimer (Forchheimer, 1901) reasoned that as the flow velocity increases, form drag becomes more prevalent. He extended Darcy's law and suggested a nonlinear relationship between the pressure drop and fluid velocity to account for the form drag effect after the Darcy regime:

$$\frac{\Delta P}{L} = \frac{\mu}{K}V + \rho CV^2 \quad (2)$$

where  $\rho$  is the density of the working fluid and  $C$  is the form drag coefficient.

Dybbs and Edwards (Dybbs and Edwards, 1984) suggested a more detailed division of the flow into Darcy, inertial flow, unsteady laminar flow and turbulent flow regimes. Bear (Bear, 1972) pointed out the existence of a pre-Darcy flow regime at the extremely low Reynolds number range. It is now widely accepted that fluid flow in porous media can be divided into

four regimes: pre-Darcy, Darcy, Forchheimer and turbulent (Fand *et al.*, 1987; Kececioglu and Jiang, 1994). The Forchheimer and turbulent regimes are often jointly termed as non-Darcy regime because the Forchheimer equation is applicable to both regimes.

The different flow behaviours in the porous media in different flow regimes can make a great difference on the heat transfer performance (Lu *et al.*, 2018). The Darcy regime is characteristic of steady laminar flow dominated by the viscous force. The heat is transferred from the near wall region to the non-near wall regions in the liquid phase through heat conduction, which is less efficient. In the Forchheimer regime, the interaction between the fluid flow and the uneven wall results in more efficient fluid mixing in the boundary layer (Dybbs and Edwards, 1984), although flow is still laminar. In the turbulent regime, velocity distribution across the pore/channel becomes more uniform because of the development of eddies and vortices, and so does the temperature in the liquid phase. The uniformly dispersed heat in the liquid phase leads to a greater temperature difference between the solid and liquid, which can greatly enhance the heat transfer performance.

The relationship between convective heat transfer coefficient and flow velocity in porous media is usually expressed in the form of empirical correlations between Nusselt ( $Nu$ ) and Reynolds ( $Re$ ) numbers. The majority of the models developed to date, e.g., by Wakao *et al.* (Wakao *et al.*, 1979) and Hwang and Chao (Hwang and Chao, 1994), are for convective heat transfer in packed beds in the form of

$$Nu = C_1 + C_2 Re^n \quad (3)$$

where  $C_1$ ,  $C_2$  and  $n$  are parameters with either constant (Wakao *et al.*, 1979) or variable (Hwang and Chao, 1994) values. This correlation works well at high  $Re$  or for fully developed flow but underestimates the heat transfer coefficient in other regimes.

Hunt and Tien (Hunt and Tien, 1988) experimentally investigated the forced convective heat transfer in a fibrous metal foam in the non-Darcy flow regime and showed that  $Nu$  was directly proportional to either the channel length based  $Re$  or the permeability based  $Re$  and that  $Nu$  depends on the porosity, pore size and thermal conductivity of the porous sample. Calmidi and Mahajan (Calmidi and Mahajan, 2000) showed that  $Nu$  in high porosity (0.89-0.97) metal foams correlated well with pore size based  $Re$  as follows

$$Nu = C_T Re^n \quad (4)$$

where  $C_T$  and  $n$  are empirical constants, varying in different  $Re$  ranges.

The porous media involved in the previous studies are largely limited to packed beds and granular porous media with porosities in the range of 0.3 – 0.5 (Fand *et al.*, 1987; Kececioglu and Jiang, 1994) or metal foams consisting of inter-connected dodecahedral-like cells with

porosities higher than 0.85 (Boomsma and Poulikakos, 2002; Dukhan *et al.*, 2014). Very little research has been conducted on convective heat transfer in porous metals manufactured by space holder methods, which have an intermediate porosity range of 0.5 - 0.8. In addition, the  $Nu-Re$  relations investigated so far are limited to the non-Darcy flow regimes. A study covering all flow regimes is necessary.

The Lost Carbonate Sintering (LCS) process (Zhao *et al.*, 2005) is one of the space holder methods used to manufacturing porous metals with highly controllable structures, including porosity, pore size, and pore shape (Zhao and Zhang, 2008). The as-manufactured porous copper can increase the convective heat transfer coefficient by 2-3 times compared with an empty channel (Xiao and Zhao, 2013; Zhang *et al.*, 2009). A recent study on the fluid flow in transparent porous glass samples mimicking the porous structures of typical porous metals manufactured by space holder methods, by micro-particle image velocimetry ( $\mu$ -PIV), has demonstrated the existence of laminar, transitional and turbulent flows and identified the flow regimes as pre-Darcy, Darcy, Forchheimer and turbulent (Lu *et al.*, 2018).

In this study, we investigated the fluid flow hydrodynamics and heat transfer performance in porous copper samples with a series of porosities, manufactured by the LCS process. We identified the flow regimes and the corresponding  $Re$  ranges and correlated the friction factor with  $Re$ . We further measured the convective heat transfer coefficients in a wide  $Re$  range and established the relationship between  $Nu$  and  $Re$  in different flow regimes. The work provides some insightful understanding of the effect of flow regimes on convective heat transfer in porous media with intermediate porosities, especially porous metals manufactured by space holder methods.

## 2. Experimental

### 2.1 Preparation of porous copper samples

Five porous copper samples, with porosities of 0.64, 0.66, 0.71, 0.75 and 0.78, were fabricated by the LCS process (Zhao *et al.*, 2005). The raw materials used in fabricating the samples were a commercially pure Cu powder (Ecka Granules Metal Powder Ltd, UK) with a mean particle size of 70  $\mu$ m and a food grade  $K_2CO_3$  powder (E&E Ltd, Australia) with a particle size range of 425 – 710  $\mu$ m. The Cu and  $K_2CO_3$  powders were mixed at a pre-specified volume ratio according to the target porosity and then compacted into a preform under a pressure of 200 MPa. The preform was first sintered at 800°C for 30 minutes to form preliminary bonding between the Cu particles and then sintered at 950°C for 2 hours to

decompose the  $K_2CO_3$  particles and form complete bonding between the Cu particles. The sample was cooled to room temperature, resulting in an open-cell porous Cu sample with a pore size of 425 – 710  $\mu m$  and a fixed porosity. The dimensions of the samples for the pressure drop and heat transfer coefficient measurements were  $20 \times 30 \times 5 \text{ mm}^3$ .

Fig. 1 shows typical SEM photographs of one of the porous copper samples at different magnifications. The majority of the pores are nearly spherical and have a size range of 425 – 710  $\mu m$ , which replicate the particles of the  $K_2CO_3$  powder used. The pores are interconnected by relatively large windows and small voids between the copper particles, allowing fluids, such as water, to flow through the sample.

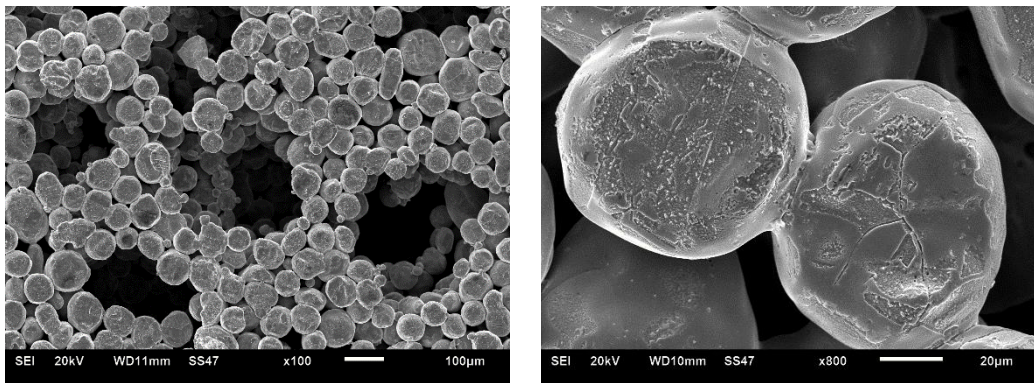


Fig. 1 SEM micrographs of an LCS porous copper sample showing representative features

## 2.2 Experimental setup

A purpose-built system was used for the heat transfer coefficient and pressure drop measurements. The experimental apparatus consisted of a test section and various supporting systems, as shown in Fig. 2. The working fluid used in this study was water. A very fine valve and a volume flow meter (FI50001A, Omega Engineering Ltd., UK) were used to control the flow rate of water passing through the porous Cu sample. The volume flow rate was calibrated for better accuracy by weighing the water flowing through the system in a fixed period of time. The maximum pressure the flow control system could apply was 400 kPa. A heater control system was used to supply electric power to the heaters and the heat flux to the test section was

varied by adjusting the voltage input. All the thermocouple and pressure transducer signals were recorded by a data logging system.

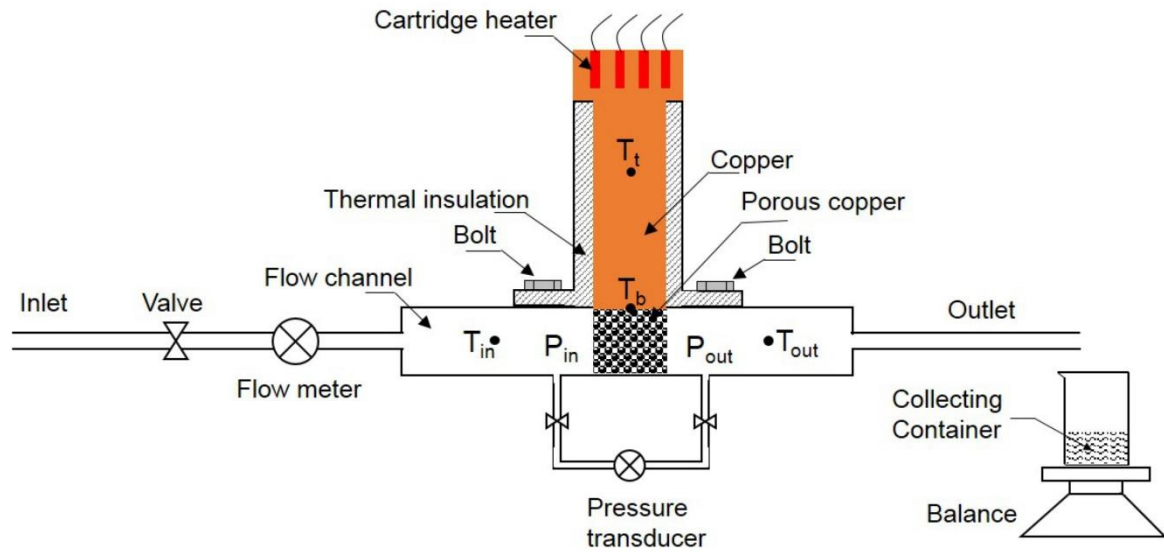


Fig. 2 Schematic of experimental setup for pressure drop and heat transfer measurements.

The porous Cu specimen was placed in a rectangular channel with the same cross-sectional area as the specimen. Five cartridge heaters were embedded in a heater block made of copper. A pure copper bar was used to transfer heat from the heater block to the specimen and to provide a more accurate measurement of the heat flux to the specimen. The heater block, copper bar and the specimen were clamped together by an aluminium jig. A thermally conductive grease with a thermal conductivity of 3.6 W/m.K was applied to the heater block/copper bar and copper bar/specimen interfaces to enhance heat conduction. The copper bar was wrapped by a thermal insulation material to reduce heat loss.

The temperature differences through the copper bar and in the water flow across the specimen were measured by four thermocouples (PT 100, Omega Engineering Ltd., UK). Two thermocouples were fixed in two holes drilled in the copper bar, one located near the copper bar/specimen interface ( $T_b$ ) and another close to the heater block ( $T_t$ ). Two thermocouples ( $T_{in}$  and  $T_{out}$ ) were fixed in the wall of the channel to measure the temperatures of the water flow on either side of the specimen. The thermocouple tips were flush with the internal wall surface to minimise disturbance to the flow.

Pressure drop across the specimen was measured by two pressure transducers across two pressure ports located 30 mm away on either side of the specimen. Three sets of pressure

transducers (DP15, Validyne Engineering, USA) with different ranges (3.5 kPa, 22 kPa and 140 kPa) were used according to the pressure drop magnitudes.

### 2.3 Measurement and calculation procedures

In each experiment, the specimen was first placed in the flow channel, which was then sealed by the heater assembly using eight bolts. Pressure drop and heat transfer coefficient were measured separately due to different flow rate steps and different times to reach steady state. Before each measurement, a high water flow rate (e.g., 1500 ml/min) was applied through the specimen for 5 minutes to flush out any air bubbles inside the specimen.

In pressure drop measurement, the flow rate was varied from low to high in steps of 50 and 200 ml/min in the flow rate ranges of 50 – 1000 and 1000 – 3000 ml/min, respectively. For each flow rate, 60 seconds was allowed for the flow to reach a steady state before recording the pressure data. The pressure recording lasted about 60 seconds at a sampling rate of 100 Hz and the mean value was used.

The heat transfer coefficient measurement was conducted immediately after the pressure drop measurement. The flow rate was varied from low to high in steps of 10, 30 and 120 ml/min in the flow rate ranges of 10 – 100, 100 – 300 and 300 – 3000 ml/min, respectively. Smaller steps were used because heat transfer coefficient was very sensitive to flow rate, especially at low flow rates. For each flow rate, the four temperatures ( $T_b$ ,  $T_t$ ,  $T_{in}$  and  $T_{out}$ ) were recorded when a steady state (temperature fluctuates  $< 0.1^\circ\text{C}$ ) was reached after 45 – 60 minutes.

The heat flux supplied to the specimen was considered to be equal to the heat flux through the copper bar by thermal conduction, if the heat loss from the copper bar is ignored, and was calculated by:

$$J = k_{Cu} A \frac{(T_t - T_b)}{d} \quad (5)$$

where  $k_{Cu}$  is the thermal conductivity of pure copper,  $A$  is the cross-sectional area of the copper bar,  $T_t$  and  $T_b$  are temperatures of the top and bottom locations, and  $d$  is the distance between  $T_t$  and  $T_b$  (110 mm).

The overall heat transfer coefficient of the cooling system, comprising the porous copper and the fluid flow, was determined by

$$h = \frac{J}{A(T_b - T_{in})} \quad (6)$$

where  $T_{in}$  is the water temperature in the inlet region.

The accuracies of the thermocouples, calliper and balance used to measure temperature, dimension and mass were 0.01°C, 0.01 mm and 0.01 g, respectively. The resultant uncertainties of heat transfer coefficient and pressure drop were estimated to be 0.6% and 0.25%, respectively, according to uncertainty analysis (Moffat, 1988).

### 3. Results and Discussion

#### 3.1 Flow behaviour

##### 3.1.1. Pressure drop

The relationship between the length-normalised pressure drop ( $\Delta P/L$ ) and the pore size based  $Re$  for porous Cu samples with different porosities are shown in Fig. 3. The pore size based  $Re$  was defined as:

$$Re = \frac{\rho V D}{\mu} \quad (7)$$

where  $\rho$  is the density of water,  $\mu$  is the dynamic viscosity of water,  $D$  is average pore size of the porous Cu samples (567.5  $\mu\text{m}$ ) and  $V$  is Darcian velocity, which is the volume flow rate of water divided by the cross-sectional area of the specimen. Fig. 3 shows that the relationship between  $\Delta P/L$  and  $Re$  is initially linear at low  $Re$  and becomes nonlinear at high  $Re$ . From the  $\Delta P/L - Re$  plots, however, it is difficult to identify the transition from the linear range to the nonlinear range.



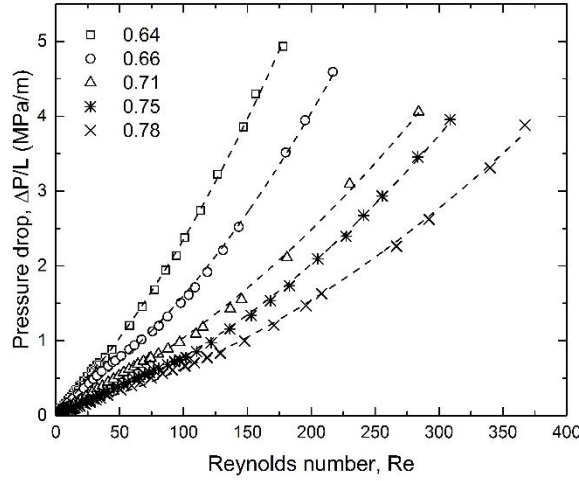


Fig. 3 Relationship between the length-normalised pressure drop and pore size based Reynolds number for porous Cu samples with different porosities.

### 3.1.2. Flow regimes

The extended Darcy-Forchheimer equation (Eq. 2) can be expressed in terms of the relationship between reduced pressure drop ( $\Delta P/LV$ ) and  $Re$  and rewritten as follows:

$$-\frac{\Delta P}{LV} = \frac{\mu}{K} + \frac{\mu C}{D} Re \quad (8)$$

Flow regime identification can be made by observing the change in the slope of the  $\Delta P/LV - Re$  plot, or the value of  $C$ . The four flow regimes, pre-Darcy, Darcy, Forchheimer and turbulent, correspond to  $C < 0$ ,  $C = 0$ ,  $C > 0$  (higher magnitude) and  $C > 0$  (lower magnitude).

Fig. 4 plots  $\Delta P/LV$  against  $Re$  for the porous Cu samples with different porosities. Five different flow regimes can be identified: (i) pre-Darcy, (ii) transition to Darcy, (iii) Darcy, (iv) transition to non-Darcy and (v) non-Darcy. The flow behaviour is similar to that reported in a previous study (Lu et al., 2018) on porous glass samples with similar porous structure as the LCS porous Cu samples. However, there are several differences between the porous Cu and the porous glass samples in terms of flow regimes. The flow in the porous glass samples showed four well-defined flow regimes: pre-Darcy, Darcy, Forchheimer and turbulent (Lu et al., 2018). The slope difference between the Forchheimer regime and the turbulent regime in the porous Cu samples is quite small. Therefore, these two flow regimes are combined and designated as non-Darcy regime in the current analysis. Fig. 4 shows that there are extended transitions from pre-Darcy to Darcy and from Darcy to non-Darcy in the porous Cu samples.

These transition regimes have a slope clearly different from the neighbouring regimes. They are also much wider than the transition regimes observed in the porous glass samples (Lu et al., 2018). In addition, the Darcy regime in the porous Cu samples occurs at a much lower  $Re$  and spans a much wider  $Re$  range than in the porous glass samples.

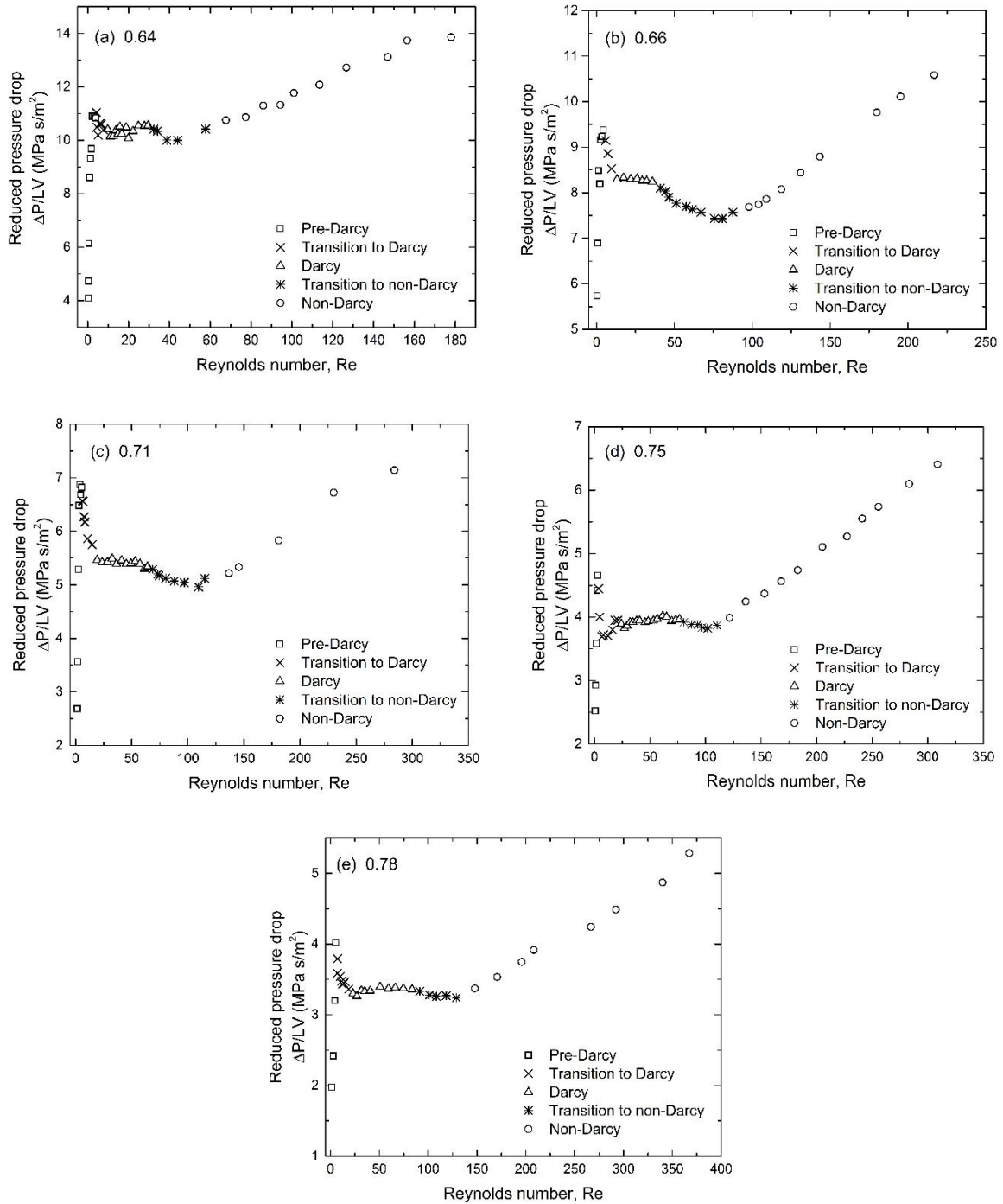


Fig. 4 Reduced pressure drop versus Reynolds number for porous Cu samples with different porosities: (a) 0.64, (b) 0.66, (c) 0.71, (d) 0.75 and (e) 0.78. Different flow regimes are distinguished by different symbols.

A pre-Darcy regime is observed in all porous Cu samples at low  $Re$  ( $< 10$ ). In the pre-Darcy regime, fluid velocity increases more rapidly than the increase in pressure gradient. Very limited information is available in the literature to explain this deviation from the Darcy linearity. One mechanism proposed by Polubarinova-Koch (Polubarinova-Koch, 2015) to explain the pre-Darcy regime is that water has a polar molecule which tends to orient itself in an electrostatic field. Static water molecules can become oriented around pore surface, forming a quasi-crystalline structure that effectively narrows the pores. As an increasing pressure gradient is applied to the water in the porous medium, the weak inter-molecular bonds are progressively overcome. In effect, the water flow channels in the porous medium are widened. The permeability of the porous medium therefore increases with water velocity until the quasi-crystalline water structure is all broken down and Darcy linearity is reached. Some researchers (Fand *et al.*, 1987; Swartzendruber, 1962) attributed the existence of the pre-Darcy regime to non-Newtonian behaviour of fluids.

A Darcy regime is evident in all porous Cu samples. Darcy regime is also called creeping flow regime as the flow is dominated by viscous forces. A purely viscous Darcy regime is identified by a horizontal line in Fig. 4, i.e., a constant  $\Delta P/LV$  value, which signifies a zero value of the second term on the right hand side of Eq. 8 and the applicability of the Darcy equation (Eq. 1). It is observed that increasing porosity leads to a later onset of Darcy regime and a wider Darcy regime.

The non-Darcy flow regime in the porous Cu samples includes the Forchheimer and turbulent regimes, which are not clearly distinguishable. As the fluid velocity increases beyond the Darcy regime, deviation from the Darcian relationship occurs. In the early stage of the Forchheimer regime, the flow within this type of porous media remains steady and laminar (Lu *et al.*, 2018). However, kinetic energy degradation begins due to pore constrictions and changes in the flow direction around the solid phase. As a consequence, both viscous and inertial drags contribute to the flow energy consumption. According to the study of Dybbs and Edwards (Dybbs and Edwards, 1984), in Forchheimer flow regime, the boundary layer begins to develop and becomes more pronounced as the flow rate increases, resulting in the formation of an “inertial core”. The non-linear relationship between pressure drop and flow rate results from these core flows outside the boundary layer. The interactions between the inertial and viscous effects lead to the deformation of the streamlines, thereby creating the non-Darcy flow regime. As the velocity increases further to a higher value, the inertial effect becomes more dominant and the flow enters into the turbulent regime.

### 3.1.3. Effect of porosity

It is observed in Fig. 3 that the pressure drop in the porous Cu samples depends strongly on the porosity of the samples. The pressure drop across the sample decreases with increasing porosity due to the lower fraction of solid matrix impeding the fluid flow and the lower tortuosity (Diao et al., 2017).

Fig. 5 shows the permeability ( $K$ ) and form drag coefficient ( $C$ ) as a function of porosity of the porous Cu samples. The permeability for the Darcy regime was obtained by fitting the experimental data within the Darcy regime to the Darcy equation (Eq. 1), while the permeability and from drag coefficient for the non-Darcy regime were obtained by fitting the experimental data within the non-Darcy regime to the extended Darcy-Forchheimer equation (Eq. 2). Fig. 5 shows that increasing porosity leads to dramatic increase in permeability and dramatic decrease in form drag coefficient. For the porous Cu sample, the permeability in the Darcy regime is approximately one third lower than the permeability in the non-Darcy regime.

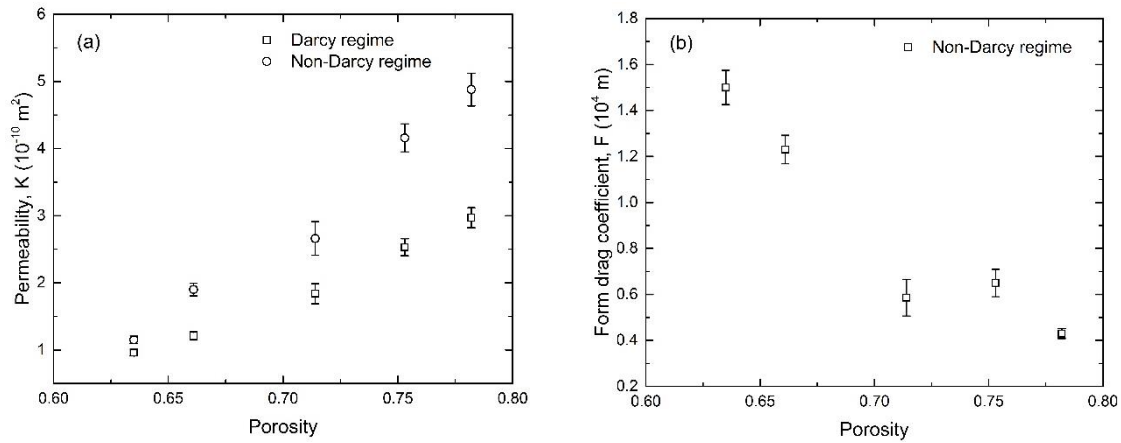


Fig. 5 Relationships of (a) permeability ( $K$ ) and (b) from drag coefficient ( $C$ ) with porosity in porous copper samples.

Fig. 6 plots the critical  $Re$  for the onset of each flow regime as a function of porosity of the porous Cu samples. The onset  $Re$  values for the transition to Darcy, Darcy, transition to non-Darcy and non-Darcy regimes are designated as  $Re_{TD}$ ,  $Re_D$ ,  $Re_{TN}$  and  $Re_{ND}$ , respectively. The ranges of  $Re$  for the five flow regimes are therefore: pre-Darcy ( $Re < Re_{TD}$ ), transition to Darcy ( $Re_{TD} < Re < Re_D$ ), Darcy ( $Re_D < Re < Re_{TN}$ ), transition to non-Darcy ( $Re_{TN} < Re < Re_{ND}$ ) and non-Darcy ( $Re > Re_{ND}$ ). Fig. 6 shows that the porosity of the porous copper sample has a

significant effect on the onset and range of the flow regimes. The onset  $Re$  for each regime increases nearly linearly with porosity. For example, non-Darcy flow starts at  $Re_{ND} = 65$  in the sample with a porosity of 0.64 and is delayed at a higher onset value of  $Re_{ND} = 150$  in the sample with a porosity of 0.78. The  $Re$  range for each regime also becomes wider with increasing porosity, especially markedly for the Darcy regime. The higher permeability and lower form drag coefficient for high porosity samples are likely the cause of the increased critical  $Re$  values, or the delayed transitions.

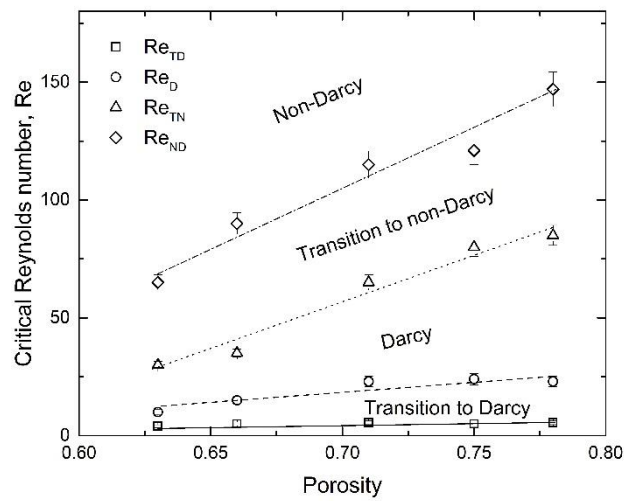


Fig. 6 Relationship between critical Reynolds numbers and porosity of the porous Cu samples.

Table 1 compares the flow regime bounds of the porous Cu samples with several porous media reported in the literature. Critical Reynolds number values are not always available for all the regime bounds in the literature. For example, Oturu et al. (2019) provided the bounds between Darcy, Forchheimer and turbulent regimes, while Boomsma and Poulikakos (2002) provided the bounds between pre-Darcy, Darcy and Forchheimer regimes. Since the experimental data on the flow regime bounds for porous metals is relatively limited, experimental data for packed sphere beds are also included for comparison. Table 1 shows that the flow regime bounds differ significantly among these porous media. However, a general trend can be observed that the onset  $Re$  for each flow regime increases with porosity, even

though the porous media have different pore morphologies and different characteristic lengths were used in defining  $Re$ .

Table 1 Reynolds number ranges of flow regimes in various porous media

Porous medium	Porosity	Pre-Darcy	Darcy	Forchheimer	Turbulent
Packed bed <sup>a</sup>	0.35	-	< 2.3	5.0 - 80	> 120
3mm spheres <sup>b</sup>	0.40	< 0.3	0.3 - 0.7	1.6 - 10	> 13
6mm spheres <sup>b</sup>	0.40	< 0.6	0.6 - 0.7	1.6 - 10	> 25
LCS porous Cu	0.64	< 4.0 (< 0.08)	10 – 30 (0.20 – 0.59)	> 65 (> 1.30)	-
	0.66	< 5.0 (< 0.10)	15 – 35 (0.33 – 0.75)	> 90 (> 1.98)	-
	0.71	< 5.5 (< 0.15)	23 – 65 (0.64 – 1.75)	> 115 (> 3.12)	-
	0.75	< 5.0 (< 0.16)	24 – 80 (0.77 – 2.56)	> 121 (> 3.87)	-
	0.78	< 5.5 (< 0.19)	23 – 85 (0.80 – 2.90)	> 147 (> 5.10)	-
Al foam 1.21 mm <sup>c</sup>	0.72	-	-	< 48	> 173
Al foam 2.75 mm <sup>c</sup>	0.75	-	-	< 100	> 500
Al foam 2.25 mm <sup>c</sup>	0.78	-	-	< 97	> 663
Al foam 450 $\mu\text{m}$ <sup>d</sup>	0.88	-	< 121	121 - 365	> 578
Al foam 10 PPI <sup>e</sup>	0.92	-	< 725	> 725	-
Al foam 20 PPI <sup>e</sup>	0.92	-	< 412	> 412	-
Al foam 40 PPI <sup>e</sup>	0.93	-	< 177	> 177	-

Notes: a. (Fand *et al.*, 1987), b. (Kececioglu and Jiang, 1994), c. (Otaru *et al.*, 2019), d. (Oun and Kennedy, 2015), e. (Boomsma and Poulikakos, 2002). The values of permeability based Reynolds number ( $\rho V \sqrt{K} / \mu$ ) are shown in brackets.

#### 3.1.4. Friction factor

The extended Darcy-Forchheimer equation (Eq. 2 or Eq. 8) can be written in another form as

$$f = \frac{D^2/K}{Re} + CD \quad (9)$$

where  $f = \frac{\Delta P}{L} \cdot \frac{D}{\rho V^2}$  is defined as friction factor. The dimensionless friction factor is therefore expected to be a function of the pore size based  $Re$ , as well as the pore size, permeability and form drag coefficient of the porous Cu sample.

Fig. 7 shows the  $f-Re$  plots for five porous Cu samples with different porosities, totalling 208 experimental data points. As expected, a higher porosity results in a lower friction factor for any given  $Re$ . It is shown that the  $f$  values calculated from Eq. 9 using the permeability values in the Darcy regime ( $C = 0$ ) fit the experimental data not only well in the Darcy regime but also reasonably well in the transition regimes before and after the Darcy regime. The deviations from the linearity are observed at very low  $Re$  values ( $< 5$ ) characterized by the pre-Darcy regime and high  $Re$  values ( $> 40 \sim 150$ , depending on porosity) characterized by the non-Darcy regime. In the non-Darcy regime, the friction factor levels off with increasing  $Re$ , because the friction factor rarely depends on  $Re$  for fully developed turbulence. This insensitivity to  $Re$  can also be understood from Eq. 9. The first term on the right hand side of Eq. 9 becomes negligible when  $Re$  becomes large, resulting in a constant friction factor.

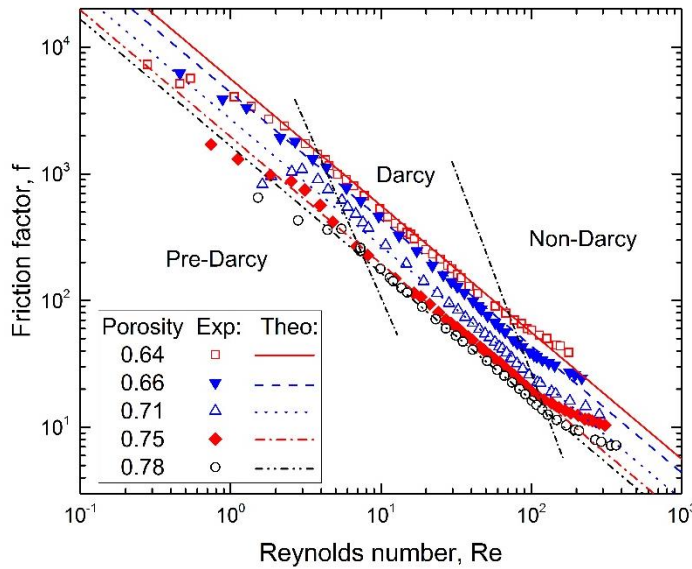


Fig. 7 Friction factor –Reynolds number plots for porous Cu samples with different porosities. The theoretical lines represent the values calculated from Eq. 9 using the permeability values in the Darcy regime ( $C = 0$ ).

### 3.2 Heat transfer performance

#### 3.2.1. Heat transfer coefficient

The convective heat transfer coefficient as a function of  $Re$  for the porous Cu samples is shown in Fig. 8. As expected, the convective heat transfer coefficient increases with increasing  $Re$ , which is proportional to the Darcian velocity or water flow rate in the present study. However, the gradient of the curves decreases gradually with increasing  $Re$ . Fig. 8 also shows that porosity has a strong effect on heat transfer performance.

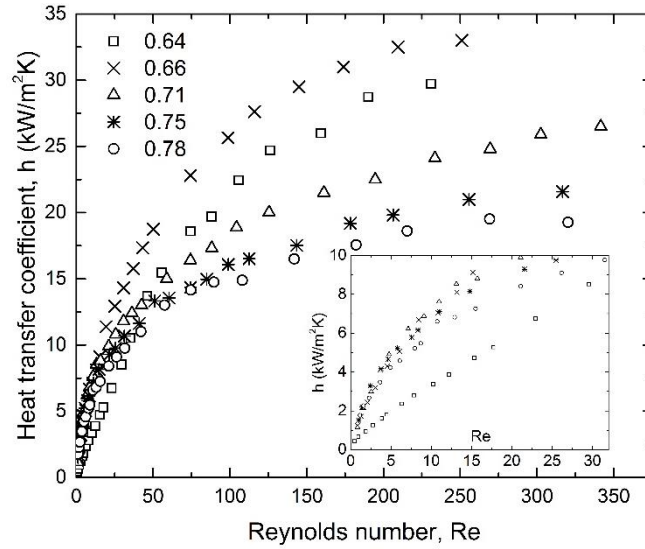


Fig. 8 Convective heat transfer coefficient versus Reynolds number for porous Cu samples with various porosities. The inset magnifies the plots in the low Reynolds number part.

#### 3.2.2. Nusselt number in different flow regimes

Fig. 9 plots  $Nu$  as a function of  $Re$  for all porous Cu samples with different porosities.  $Nu$  was calculated from the convective heat transfer coefficient as follows:

$$Nu = \frac{hL}{k_f} \quad (10)$$

where  $h$  is the convective heat transfer coefficient,  $L$  is the length of the heated section of the porous copper in the mean flow direction and  $k_f$  is the thermal conductivity of fluid, i.e. water in the present study.



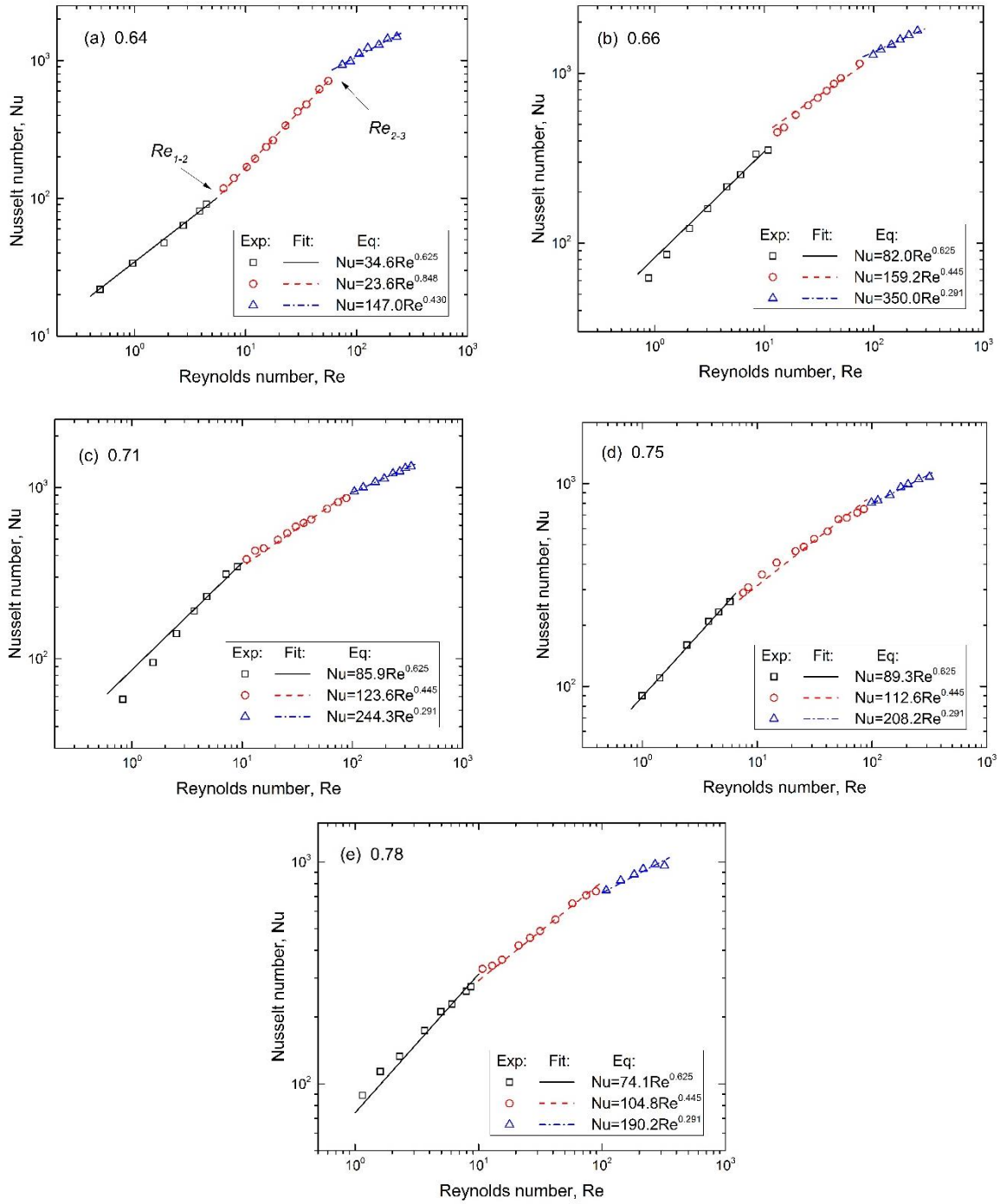


Fig. 9 Nusselt number as a function of Reynolds number for porous Cu samples with different porosities: (a) 0.64, (b) 0.66, (c) 0.71, (d) 0.75 and (e) 0.78. The data can be correlated by Eq. (4) in three sections.

Fig. 9 shows that each plot can be divided into three sections, with each section fitting well with Eq. (4). The slope of the fitted lines, i.e. the exponent  $n$  (Table 2), decreases from the first section (low  $Re$ ) to the second section (medium  $Re$ ) and further to the third section (high  $Re$ ), except the sample with a porosity of 0.64, in which  $n$  increases from the first section to the second section. Although the three sections for each plot have different relations, the value of the exponent  $n$  for each section tends to be a constant for all porous Cu samples except the one with a porosity of 0.64. In other words,  $n$  is largely independent of porosity, except at the relatively low porosity of 0.64.

Table 2 Exponent  $n$  values for different sections of  $Nu - Re$  plots.

Porosity	First section (low $Re$ )	Second section (medium $Re$ )	Third section (high $Re$ )
0.64	0.625	0.848	0.430
0.66, 0.71, 0.75 and 0.78	0.625	0.445	0.291

The value of  $n$  depends not only on the flow state (flow regime) but also on the porous structure. In packed beds, the reported values of  $n$  were 0.6 (Wakao *et al.*, 1979) and 1.35 ( $Re < 100$ ) and 1.04 ( $Re > 100$ ) (Hwang and Chao, 1994), depending on the particle sizes used. In sintered fibrous media, the value was found to be 1 (Hunt and Tien, 1988). In high porosity metal foams, the value was 0.5 (Calmidi and Mahajan, 2000). In comparison, the LCS porous Cu has  $n$  values ranging from 0.29 to 0.85, depending mainly on flow regime.

### 3.2.3. Effect of porosity

Fig. 10 shows the variations of heat transfer coefficient with porosity at various  $Re$  values, or flow rates. The effect of porosity on heat transfer coefficient is dependent on the flow rate. At low flow rates ( $Re < 10$ ), all samples have a similar heat transfer coefficient except the sample with a porosity of 0.64, which has a lower heat transfer coefficient (see the inset in Fig. 8). At high flow rates ( $Re > 30$ ), the heat transfer coefficient first increases with increasing porosity from 0.64 to 0.66 and then decreases with increasing porosity further.

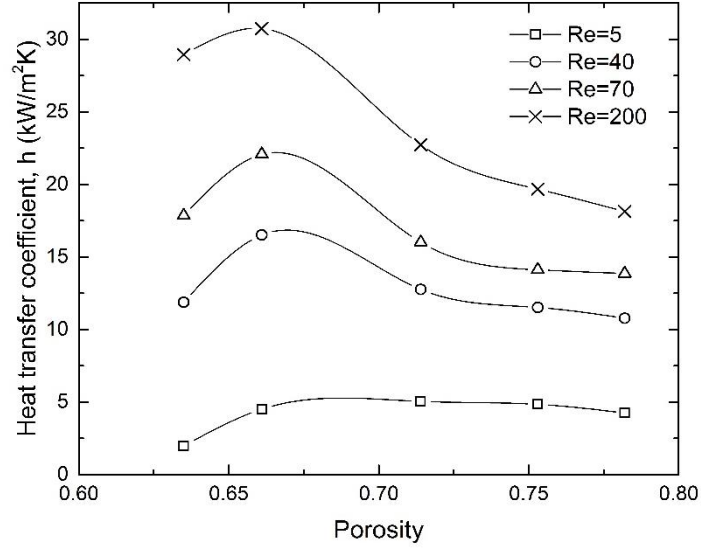


Fig. 10 Convective heat transfer coefficient versus porosity at various Reynolds numbers.

Fig. 11 shows the variations of the correlation parameter  $C_T$  with porosity for the first, second and third sections identified in Fig. 9. The trend is similar to that displayed in Fig. 10. At low flow rates ( $Re < 10$ , first section), all samples have a similar  $C_T$  value except the 0.64 porosity sample. At high flow rates ( $Re > 30$ , second and third sections),  $C_T$  first increases with increasing porosity from 0.64 to 0.66 and then decreases with increasing porosity further.

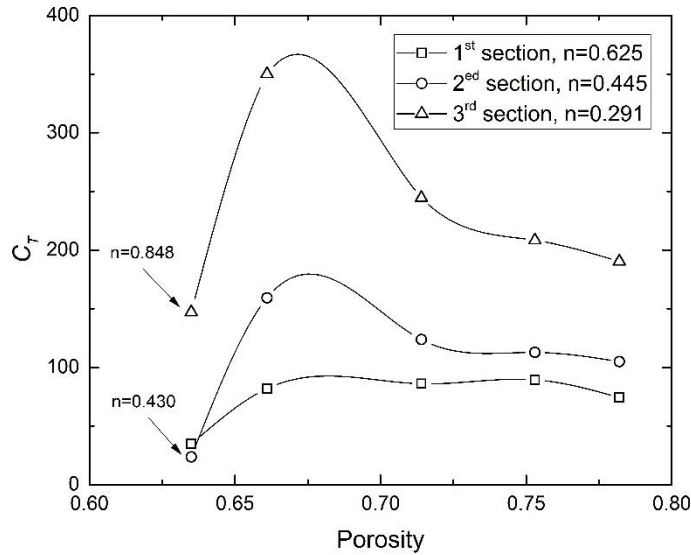


Fig. 11 Correlation parameter  $C_T$  versus porosity for first, second and third sections.

The effect of porosity on heat transfer coefficient or  $Nu$  can be understood by considering heat conduction through the solid matrix and heat convection in the fluid flow. Either conduction or convection can be the main factor limiting the overall heat transfer. Conduction is largely determined by porosity, with the thermal conductivity approximately proportional to  $(1 - \varepsilon)^2$  according to (Ashby et al., 2000; Thewsey and Zhao, 2008). Convection is not only dependent on porosity, e.g., related to  $\varepsilon/(1 - \varepsilon)$  in packed beds (Walker and Glover, 2010), but also affected by flow rate. The heat transfer performance depends on the coupled effect of porosity and flow rate.

At very low flow rates ( $Re < 10$ ), the convective heat transfer at the solid-fluid interface would be the limiting factor. Increasing porosity can increase convection through the fluid, because of the increased amount of fluid, and therefore can increase overall heat transfer in the porous media. However, the heat transfer from the near wall layer to the centre core within the fluid flow is mainly through conduction because of no wakes or vortices to help transfer heat. Therefore, increasing porosity beyond a certain level has no major influence on the convective heat transfer.

At high flow rates ( $Re > 10$ ), either conduction in the solid matrix or convection in the fluid flow can be the limiting factor. The samples with a low porosity have a superior thermal conductivity due to the high proportion of solid matrix (Thewsey and Zhao, 2008). However, they have low internal surface area and low fluid permeability (Diao *et al.*, 2015), which reduce the convective heat transfer from the solid to the coolant. The overall heat transfer coefficient or  $Nu$  is limited by the convection contribution and can be low. Conversely, although the samples with a high porosity have good convective heat transfer from the solid to the coolant and by the moving coolant, they have poor thermal conductivity, which limits the overall heat transfer. As thermal conductivity decreases exponentially with porosity, the overall heat transfer coefficient or  $Nu$  decreases rapidly with porosity.

Figs. 10 and 11 suggest that the optimum porosity to give the best heat transfer performance is 0.66 in the current research. At this critical porosity, heat conduction through the solid matrix matches heat convection in the fluid flow, resulting in the best overall heat transfer performance.

#### 3.2.4. Critical Reynolds numbers

Fig. 12 shows the values of the critical  $Re$  for the flow regimes and for the three sections of the  $Nu-Re$  curve identified in Fig. 9, as a function of porosity. The critical  $Re$  values

corresponding to the transitions from the first section to the second section and from the second to the third are designated as  $Re_{1-2}$  and  $Re_{2-3}$ , respectively. It is shown that  $Re_{1-2}$  falls within the transition-to-Darcy regime ( $Re_{TD} - Re_D$ ), while  $Re_{2-3}$  falls within the transition-to-non-Darcy regime ( $Re_{TN} - Re_{ND}$ ). It can be concluded that the fluid flow behaviour plays an important role in determining the heat transfer performance of the porous Cu samples. The three sections of the  $Nu-Re$  curves broadly correspond to the pre-Darcy, Darcy and non-Darcy regimes.

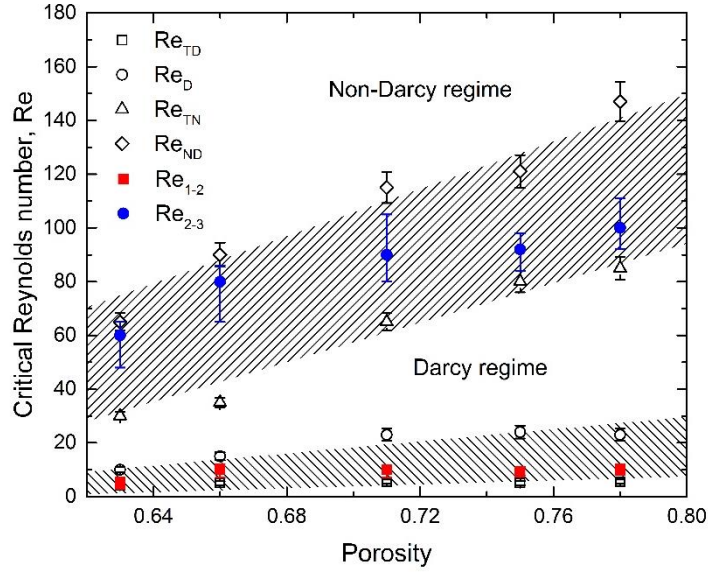


Fig. 12 Critical Reynolds numbers for flow regimes ( $Re_{TD}$ ,  $Re_D$ ,  $Re_{TN}$  and  $Re_{ND}$ ) and for  $Nu-Re$  sections ( $Re_{1-2}$  and  $Re_{2-3}$ ) as a function of porosity. The patterned areas show the transition flow regimes.

#### 4. Conclusions

- 1) Five flow regimes, namely pre-Darcy, transition to Darcy, Darcy, transition to non-Darcy and non-Darcy, have been identified from the  $\Delta P/LV - Re$  plots. The  $Re$  values for the flow regime boundaries increased nearly linearly with porosity.
- 2) The permeability increased and form drag coefficient decreased with increasing porosity of the porous Cu samples. The friction factor decreased dramatically with flow rate.
- 3) The heat transfer coefficient of the porous Cu samples depended strongly on the flow rate. The Nu-Re curves had three sections, with each followed the correlation  $Nu = C_T Re^n$  with different  $C_T$  and  $n$  values. The value of  $n$  was largely independent of porosity, except at the relatively low porosity of 0.64.
- 4) The flow regimes had a strong effect on the heat transfer performance. The three sections of the Nu-Re curves broadly corresponded to the pre-Darcy, Darcy and non-Darcy regimes.

#### Acknowledgment

This work has been supported by the Engineering and Physical Sciences Research Council (Grant No. EP/N006550/1). X. K. Lu would like to thank the University of Liverpool and the Chinese Scholarship Council for a PhD studentship.

## Nomenclature

$A$	cross-sectional area of the sample (m <sup>2</sup> )
$C$	form drag coefficient (m)
$C_1, C_2, C_T$	constants
$D$	average pore size (m)
$d$	distance (m)
$F$	form drag coefficient
$f$	friction factor
$h$	heat transfer coefficient (kW/m <sup>2</sup> K)
$J$	heat flux (W)
$K$	permeability (m <sup>2</sup> )
$k_{Cu}$	thermal conductivity of copper (W/m K)
$k_f$	thermal conductivity of water (W/m K)
$L$	length of sample (m)
$L_c$	length of channel (m)
$Nu$	Nusselt number
$n$	exponent
$Re$	Reynolds number
$Re_{TD}$	onset of transition to Darcy regime
$Re_D$	onset of Darcy regime
$Re_{TN}$	onset of transition to non-Darcy regime
$Re_N$	onset of non-Darcy regime
$T_b$	temperature of copper bar, bottom (K)
$T_t$	temperature of copper bar, top (K)
$T_{in}$	temperature of inlet water (K)
$T_{out}$	temperature of outlet water (K)
$V$	Darcian velocity (m/s)

## Greek symbols

$\Delta P$	pressure drop (kPa)
$\mu$	fluid viscosity (Pa s)
$\rho$	fluid density (kg/m <sup>3</sup> )

## References

- Ashby, M.F., Evans, T., Fleck, N.A., Hutchinson, J., Wadley, H., Gibson, L., 2000. Metal foams: a design guide. Elsevier.
- Bear, J., 1972. Dynamics of fluids in porous media—American Elsevier pub. Comp., inc. New York, 764p.
- Bejan, A., 2013. Convection heat transfer. John Wiley & sons.
- Boomsma, K., Poulikakos, D., 2002. The effects of compression and pore size variations on the liquid flow characteristics in metal foams. *Journal of fluids engineering* 124, 263-272.
- Calmidi, V., Mahajan, R., 2000. Forced convection in high porosity metal foams. *Journal of heat transfer* 122, 557-565.
- Diani, A., Bodla, K.K., Rossetto, L., Garimella, S.V., 2015. Numerical investigation of pressure drop and heat transfer through reconstructed metal foams and comparison against experiments. *International Journal of Heat and Mass Transfer* 88, 508-515.
- Diao, K., Zhang, L., Zhao, Y., 2017. Measurement of tortuosity of porous Cu using a diffusion diaphragm cell. *Measurement* 110, 335-338.
- Diao, K.K., Xiao, Z., Zhao, Y.Y., 2015. Specific surface areas of porous Cu manufactured by Lost Carbonate Sintering: Measurements by quantitative stereology and cyclic voltammetry. *Materials Chemistry and Physics* 162, 571-579.
- Dukhan, N., Bağcı, Ö., Özdemir, M., 2014. Metal foam hydrodynamics: Flow regimes from pre-Darcy to turbulent. *International Journal of Heat and Mass Transfer* 77, 114-123.
- Dybbbs, A., Edwards, R.V., 1984. A New Look at Porous Media Fluid Mechanics — Darcy to Turbulent, in: Bear, J., Corapcioglu, M.Y. (Eds.), *Fundamentals of Transport Phenomena in Porous Media*. Springer Netherlands, Dordrecht, pp. 199-256.
- Fand, R., Kim, B., Lam, A., Phan, R., 1987. Resistance to the flow of fluids through simple and complex porous media whose matrices are composed of randomly packed spheres. *J. Fluids Eng* 109, 268-274.
- Forchheimer, P., 1901. Wasserbewegung durch boden. *Z. Ver. Deutsch, Ing.* 45, 1782-1788.
- Goodall, R., Mortensen, A., 2014. 24 - Porous Metals, in: Laughlin, D.E., Hono, K. (Eds.), *Physical Metallurgy* (Fifth Edition). Elsevier, Oxford, pp. 2399-2595.
- Hetsroni, G., Gurevich, M., Rozenblit, R., 2006. Sintered porous medium heat sink for cooling of high-power mini-devices. *International Journal of Heat and Fluid Flow* 27, 259-266.
- Hunt, M.L., Tien, C.L., 1988. Effects of thermal dispersion on forced convection in fibrous media. *International Journal of Heat and Mass Transfer* 31, 301-309.
- Hwang, G., Chao, C., 1994. Heat transfer measurement and analysis for sintered porous channels. *Journal of heat transfer* 116, 456-464.
- Kececioglu, I., Jiang, Y., 1994. Flow through porous media of packed spheres saturated with water. *J. Fluids Eng* 116, 164-170.
- Lu, X., Zhao, Y., Dennis, D.J.C., 2018. Flow measurements in microporous media using micro-particle image velocimetry. *Physical Review Fluids* 3, 104202.
- Moffat, R.J., 1988. Describing the uncertainties in experimental results. *Experimental Thermal and Fluid Science* 1, 3-17.
- Nie, Z., Lin, Y., Tong, Q., 2017. Numerical investigation of pressure drop and heat transfer through open cell foams with 3D Laguerre-Voronoi model. *International Journal of Heat and Mass Transfer* 113, 819-839.
- Otaru, A., Morvan, H., Kennedy, A., 2019. Airflow measurement across negatively infiltration processed porous aluminum structures. *AIChE Journal* 65, 1355-1364.
- Oun, H., Kennedy, A., 2015. Tailoring the pressure-drop in multi-layered open-cell porous inconel structures. *Journal of Porous Materials* 22, 1627-1633.
- Polubarinova-Koch, P.I., 2015. Theory of ground water movement. Princeton University Press.



Swartzendruber, D., 1962. Non - Darcy flow behavior in liquid - saturated porous media. *Journal of Geophysical Research* 67, 5205-5213.

Thewsey, D.J., Zhao, Y.Y., 2008. Thermal conductivity of porous copper manufactured by the lost carbonate sintering process. *physica status solidi (a)* 205, 1126-1131.

Wakao, N., Kaguei, S., Funazkri, T., 1979. Effect of fluid dispersion coefficients on particle-to-fluid heat transfer coefficients in packed beds: Correlation of nusselt numbers. *Chemical Engineering Science* 34, 325-336.

Walker, E., Glover, P.W., 2010. Permeability models of porous media: Characteristic length scales, scaling constants and time-dependent electrokinetic coupling. *Geophysics* 75, 235-246.

Xiao, Z., Zhao, Y., 2013. Heat transfer coefficient of porous copper with homogeneous and hybrid structures in active cooling. *Journal of Materials Research* 28, 2545-2553.

Zhang, L., Mullen, D., Lynn, K., Zhao, Y., 2009. Heat Transfer Performance of Porous Copper Fabricated by Lost Carbonate Sintering Process. *MRS Online Proceedings Library Archive* 1188.

Zhao, Y.Y., Fung, T., Zhang, L.P., Zhang, F.L., 2005. Lost carbonate sintering process for manufacturing metal foams. *Scripta Materialia* 52, 295-298.

Zhao, Y.Y., Zhang, L.P., 2008. Fabrication of high melting-point porous metals by lost carbonate sintering process via decomposition route. *Proceedings of the Institution of Mechanical Engineers, Part B: Journal of Engineering Manufacture* 222, 267-271.